Multidecadal variability in the transmission of ENSO signals to the Indian Ocean

G. Shi,[1] J. Ribbe,[1] W. Cai,[2,3] T. Cowan[2,3]

Ge Shi, CSIRO Atmospheric Research, PMB 1, Aspendale, Victoria 3195, Australia. (ge.shi@csiro.au)

[1]Department of Biological and Physical Sciences, University of Southern Queensland, Queensland, Australia. (ge.shi@csiro.au)

[2]CSIRO Marine and Atmospheric Research, PMB 1, Aspendale, Victoria 3195, Australia.

[3]Wealth from Oceans Flagship, CSIRO, PO Box 120, Cleveland, Queensland 4163, Australia.

Since 1980, transmission of El Niño-Southern Oscillation (ENSO) signals into the Indian Ocean invloves an equatorial, and a subtropical North Pacific (NP) Rossby wave pathway. We examine the robustness of the amount of energy that leaves the Pacific via each of the pathway using the Simple Ocean Data Assimilation with the Parallel Ocean Program (SODA-POP) reanalysis and a multi-century coupled model control experiment. We find that in the pre-1980 period, little ENSO signal is transmitted to the Indian Ocean and does not involve the subtropical NP pathway. Such multidecadal variability is periodically produced by the climate model. Examinations reveal that when ENSO is weak as determined by Niño3.4, their meridional extent is narrow, the associated discharge-recharge does not involve the subtropical NP pathway; further, weak ENSO events have a low signal-to-noise ratio, making the transmission hard to detect. The dynamics of multidecadal variability in ENSO strength awaits further investigation.

1. Introduction

Pacific Ocean variability is known to transmit to the Indian Ocean. The consensus is that variations in zonal Pacific equatorial winds force a response primarily along the Western Australia (WA) coast [*Clarke*, 1991; *Meyers*, 1996; *Masumoto and Meyers*, 1998; *Potemra*, 2001; *Wijffels and Meyers* 2004; *Cai et al.*, 2005a]. The energy off the WA coast arises from equatorial Rossby waves generated by zonal wind anomalies in the central equatorial Pacific which become coastally trapped waves where the New Guinea coast intersects the Pacific equator. In addition to the equatorial pathway, *Cai et al.* [2005a] found an off-equatorial pathway: using an updated thermal analysis covering over 20 years since 1980 from the Australian Bureau of Meteorology Research Center (BMRC) [*Smith*, 1995], they showed that subtropical NP Rossby waves associated with ENSO impinge on the western boundary and move equatorward along the pathway of Kelvin-Munk waves [*Godfrey*, 1975], and reflect as equatorial Kelvin waves. The reflected Kelvin waves impinge on the Australasian continent and move poleward along the northern WA coast as coastally-trapped waves, radiating Rossby waves into the south Indian Ocean. *Cai et al.* [2005a] showed that some 55% of the total interannual variance of the WA thermocline is linked to the subtropical NP Rossby waves and participate in the ENSO recharge-discharge [*Jin*, 1997; *Meinen and McPhaden*, 2000]. Here we examine the robustness of the amount of energy transmission via each of the pathway in the pre-1980 period and find that there are significant differences to the post-1980 period. We then examine the presence of such multidecadal variability in a coupled climate model.

2. Data and Method

We utilize the newly available reanalysis of SODA-POP (version 1.4.2) [*Carton and Giese*, 2006]. The new model product uses the European Center for Medium Range Forecasts ERA-40 atmospheric reanalysis winds. It has a spatial resolution of 0.5° latitude by 0.5° longitude grid, and covers a period from 1958 to 2001. Both the SODA-POP and BMRC reanalyses independently incorporated Expendable Bathythermograph profiles and time-series from the Tropical Atmosphere Ocean buoy array [*McPhaden et al.*, 1998]. We find that there are remarkable differences in the transmission between the pre- and post-1980 periods. To examine the robustness of such multidecadal variability, we take outputs of a multi-century control experiment with the new CSIRO coupled climate model (version 3.5). The new version simulates a more realistic transmission process, although it still suffers from the common cold tongue bias, i.e., the equatorial Pacific cold tongue extends too far west. The ENSO frequency is reasonably simulated as reported earlier [*Cai et al.*, 2004], but the amplitude is too large. Despite these deficiencies the model produces similar multidecadal variations in the transmission.

3. ENSO cycle and transmission into the Indian Ocean in the pre- and post-1980 period

Figure 1 displays the lag-correlation between Niño3.4 and $D20$ at various lags for the post-1980 (left column) and pre-1980 (right column) from SODA-POP. The ENSO cycle is well simulated in both periods but with noticeable differences. The meridional extent is narrower in the pre-1980 period. This difference, and the feature of stronger ENSO since 1980, have been observed by previous studies [*Wang*, 1995; *Wallace et al.*, 1998; *Wang* *and An*, 2001]. A central difference is that little signal is transmitted into the Indian Ocean in the pre-1980 period.

In the post-1980 period (left column), 9 months prior to the peak of an El Niño, the pattern in the equatorial Pacific (5°S- 5°N) shows a recharged phase, but an off-equatorial upwelling Rossby wave (indicated by negative contours) develops and radiates from the eastern boundary, and is reinforced in the vicinity of (155°W, 17°N). After a strong growth en-route westward, it impinges on the western boundary, moves equatorward and then reflects back as an equatorial Kelvin wave (Lag -3). The reflected Kelvin wave then forces a coastally-trapped wave, which propagates poleward along the WA coast, contributing to a discharged phase of an El Niño at Lag 0. The discharge off the WA coast reaches a maximum approximately three months after an El Niño peaks (Lag +3). Thus some of the signal along the central WA coast can be traced to the subtropical NP. This is the subtropical NP pathway described by *Cai et al.* [2005a] and SODA-POP simulates this well. The phase speed of the off-equatorial Rossby waves is far faster than that of observed Rossby waves [*Chelton and Schlax*, 1997; *Cipollini et al.*, 2001]; however, these waves are not free Rossby waves but are strongly controlled by wind anomalies or by the atmosphere-ocean coupling [*Cai et al.*, 2005a].

Rossby waves in the pre-1980 period are closer to the equator, mostly within about 10°S-10°N. As a result, there is little transmission via the subtropical NP pathway. This is further illustrated in Fig. 2, which shows lag correlation between $D20$ at the NP western boundary (Philippine Sea (PS) box, 120°E-125°E, 12.5°N-17.5°N) and $D20$ everywhere. To compare with Fig. 1, the PS $D20$ is sign-reversed so that a discharge signal is represented by negative correlations. Rossby wave propagation is seen in both periods, but in the post-1980 period (left column), there are strong coherence between ENSO and NP Robbsy waves and clear signal transmission to the WA coast; these features are virtually absent in the pre-1980 period (right column).

Does the energy leave the Pacific Ocean via the equatorial pathway in the pre-1980 period? We conduct a lag-correlation analysis of $D20$ anomalies with time series of $D20$ anomalies averaged over a central WA box (112°E-120°E, 15°S-22°S) (Fig. 3). To compare with Fig. 1, the WA $D20$ is sign-reversed. Maximum discharge off the WA coast appears at Lag 0, and at Lag -3 it corresponds to an El Niño peak (at Lag 0 in Fig. 1).

For the post-1980 period (left column, Fig. 3) there is a strong similarity between Fig. 1 and Fig. 3, and the WA anomaly is predominantly generated by ENSO processes. In the pre-1980 period (right column, Fig. 3), the evolution is vastly different. There is little correlation between WA $D20$ and anomalies elsewhere at most lags, except at Lag -6, when weak but significant correlations exist in the western equatorial Pacific. Corresponding maps of correlation with zonal winds also show a maximum in the western equatorial Pacific at Lag -6, implying that some Pacific signals do propogate through the equatorial pathway. Nevertheless, the overall lack of correlation suggests that in the pre-1980 period the transmission via the equatorial pathway is so weak that it does not manifest above the stochastic noise.

What we have described above is the difference of the statistical properties between the two periods. Within each period, the proportion of energy transmission via each pathway varies significantly from one event to another; for example, in the 1997 event, transmission via the NP pathway is smaller than that via the equatorial pathway. Despite this, it is rather significant that the statistical property of events over one 20-year period is so different from that over another 20-year period, highlighting the existence of an underlying mechanism.

The thermocline in the Pacific Ocean has been changing on decadal timescales, and could have affected the Indian Ocean [markcite*McPhaden and Zhang*, 2002; markcite*Annamalai et al.*, 2005]. This is supported by our results: the stronger post-1980 ENSO discharge signals contribute to a shallowing thermocline in the southern tropical Indian Ocean (figure not shown) and could affect the development of the Indian Ocean Dipole (IOD), by pre-conditioning a shallower thermocline [markcite*Annamalai et al.*, 2005] as the associated stronger easterly anomalies lift the thermocline. These might explain the better defined IOD pattern during the post-1980 period (Fig. 1, lowest panel).

4. The dynamics

Pre-1980 ENSO events are weaker and have a narrower meridional extent than the post-1980 ENSOs (Fig. 1) [*Wang*, 1995]. Does such multidecadal variability in the ENSO properties contribute to the difference in the pre- and post-1980 transmission? We take outputs of the new CSIRO multi-century control experiment and examine if similar multidecadal variations exist. Time series of WA $D20$ and Niño3.4 are constructed from the coupled model outputs and a 20-year sliding window is used to calculate the correlation between them at Lags +3 and +6 (Fig. 4, black and blue curve). We calculated more than one lag in case the model transmission signal does not peak at exactly the same time as in SODA-POP. The model transmission undergoes similar multidecadal fluctuations:

in some 20-year periods the correlation is not significant, i.e., little is transmitted or generated; in other periods the correlation reaches as high as 0.8. We then calculate a time series of standard deviation of Niño3.4 using a 20-year sliding window (red curve, Fig. 4). The amplitude fluctuates significantly, between about 0.6°C and 1.1°C. The central point is that a strong correlation exists between the standard deviation curve (red) and the Lag +3 curve (black) with a correlation of 0.79: a strong transmission is seen when ENSO events are strong, and vice versa.

Maps of correlation (not shown) between Niño3.4 and $D20$ everywhere and between the WA $D20$ and $D20$ everywhere for the strong (centered at year 315) and weak (centered at year 215) transmission periods resemble those of Figs. 1 and 3 for the post- and pre-1980 periods, respectively. For the weak transmission period (year 215), there is little involvement of the subtropical NP pathway and the meridional extent of the ENSO anomaly is narrower. These contrasts are also reflected in maps of one-standard deviation anomaly patterns of SST and surface wind associated with ENSO for the strong (left column, Fig. 4) and weak (right column, Fig. 4) transmission periods, reminiscent of the difference between the post- and pre-1980 periods in SODA-POP.

During strong-ENSO periods, the tropical Indo-Pacific system is overwhelmed by ENSO signals, therefore the ratio of "ENSO signal to stochastic noise" is greater than that during weak-ENSO periods. To illustrate this, we define signal as the standard deviation associated with the Niño3.4, determined from a linear regression onto the Niño3.4 index, and noise as the standard deviation of the residual after removing ENSO signals. Maps of such ratios for $D20$ for SODA-POP and the coupled model are displayed in Fig. 5. The ratios are generally much larger for the strong-ENSO periods. The results are therefore consistent with the multidecadal variation of the Indo-Pacific teleconnection depicted in Figs. 1-4, and provide an explanation as to why in weak-ENSO periods a transmission signal might not manifest itself above stochastic noises.

5. Conclusions

Based on data since 1980, ENSO discharge-recharge signals are believed to transmit into the Indian Ocean arriving mainly at the WA coast via an equatorial pathway, and a subtropical NP pathway, The present study examines the robustness of energy leaving the Pacific via these pathways. Using SODA-POP, we find that in the pre-1980 period, little ENSO signal is transmitted to the Indian Ocean. The lack of transmission results from two interconnected factors: firstly, the NP pathway is not involved because of a narrower meridional extent of ENSO; secondly, the ENSO events are weaker leading to smaller transmission signals via the equatorial pathway that are drowned under stochastic noise. A multi-century coupled climate model experiment reproduces these features, confirming that these are not artefacts of the reanalysis system. The presence of these multidecadal fluctuations in our model without climate change forcing suggests that the stronger discharge in the post-1980 may not be green-house induced. The dynamics that drive the multidecadal fluctuations of ENSO properties need to be investigated, and this will be pursued in another paper.

Acknowledgments. We thank Neville Smith and SODA-POP group for the permission to use their reanalysis data. W. Cai and T. Cowan are also supported by the Australian Greenhouse Office.

References

Annamalai, H., J. Potemra, R. Murtugudde, and J. P. McCreary (2005), Effect of Preconditioning on the Extreme Climate Events in the Tropical Indian Ocean. *J. Climate*, *18*, 3450-3469.

Cai, W. J., G. Meyers, and G. Shi (2005a), Transmission of ENSO signal to the Indian Ocean. *Geophys. Res. Lett.*, *32*, L05616, doi:10.1029/2004GL021736.

Cai, W. J., H. H. Hendon, and G. Meyers (2005b), An Indian Ocean Dipole in the CSIRO coupled climate model. *J. Climate*, *18*, 1449–1468.

Cai, W. J., J. M. McPhaden, and M. A. Collier (2004), Multidecadal fluctuations in the relationship between equatorial Pacific heat content anomalies and ENSO amplitude. *Geophys. Res. Lett.*,*31*, L01201, doi:10.1029/2003GL018714.

Carton, J. A., and S. B. Giese (2006), SODA: A Reanalysis of Ocean Climate. *Mon. Wea. Rev.* , submitted.

Chelton, D. B., and M. G. Schlax (1996), Global Observations of Oceanic Rossby Waves. *Science*, *272*, 234–238.

Cipollini, P., D. Cromwell, P. G. Challenor, and S. Raffaglio (2001), Rossby waves detected in global ocean colour data. *Geophys. Res. Lett.*, *28*, 323–326.

Clarke, A. J. (1991), On the reflection and transmission of low-frequency energy at the irregular western Pacific Ocean boundary. *J. Geophys. Res.*, *96*, 3289–3305.

Godfrey, J. S. (1975), On ocean spindown I: A linear Experiment. *J. Phys. Oceanogr.*, *5*, 399–409.

Jin, F.-F. (1997), An equatorial ocean recharge paradigm for ENSO. Part I: Conceptual model. *J. Atmos. Sci.*, *54*, 811–829.

Masumoto, Y., and G. Meyers (1998), Forced Rossby waves in the southern tropical Indian Ocean. *J. Geophys. Res.*, *103*, 27589–27602.

McPhaden, M. J., and D. X. Zhang (2002), Slowdown of the meridional overturning circulation in the upper Pacific Ocean. *Nature*, *415*, 603-608.

McPhaden, M. J., and Coauthors (1998), The Tropical Ocean Global Atmosphere (TOGA) observing system: A decade of progress. *J. Geophys. Res., 103,* 14 169–14 240.

Meinen, C. S., and M. J. McPhaden (2000), Observations of warm water volume changes in the equatorial Pacific and their relationship to El Niño and La Niña. *J. Climate*, *13*, 3551–3559.

Meyers, G. (1996), Variation of the Indonesian Throughflow and the El Niño Southern Oscillation, *J. Geophys. Res.*, *101*, 12255–12263.

Potemra, J. T. (2001), Contribution of equatorial Pacific winds to southern tropical Indian Ocean Rossby waves. *J. Geophys. Res.*, *106*, 2407–2422.

Smith, N. R. (1995), The BMRC ocean thermal analysis system. *Aust. Meteor. Mag., 44*, 93–100.

Wallace, J. M., E. M. Rasmusson, T. P. Mitchell, V. E. Kousky, E. S. Sarachik, and H. von Storch (1998), On the structure and evolution of ENSO-related climate variability in the tropical Pacific: lessons from TOGA. *J. Geophys. Res.,* 103, 1424114259.

Wang, B. (1995), Interdecadal Changes in El Nino Onset in the Last Four Decades. *J. Climate*, *8,* 267–285.

Wang, B., and S. I. An (2001), Why the properties of El Nino changed during the late 1970s. *Geophys. Res. Lett.*, 28, 3709–3712.

Wijffels, S., and G. Meyers (2004), An Intersection of oceanic wave guides: Variability in the Indonesian Throughflow Region. *J. Phys. Oceanogr.*, *34*, 1232–1253.

Figure 1. Outputs from the SODA-POP reanalysis (Version 1.4.2), showing correlation between Niño3.4 and gridpoint $D20$ at various lags with a 3-month interval. Positive correlations imply deeper depths, and negative lags mean the Niño3.4 lags. Left column is for the post-1980 and right column for the pre-1980 period. A value of 0.28 indicates statistical significance at 95% confidence level.

Figure 2. The same as Figure 1, but with time series of $D20$ in a Philippine Sea (PS) box (120°E-125°E, 12.5°N-17.5°N). To show discharge signals the PS $D20$ is sign-reversed before analysis for comparisons with Figure 1.

Figure 3. The same as Figure 1, but with time series of $D20$ averaged over a central WA box (112°E-120°E, 15°S-22°S). To show discharge signals the WA $D20$ is sign-reversed before analysis for comparisons with Figure 1.

Figure 4. Coupled model results: a), time series of correlation between Niño3.4 and the WA $D20$ at Lags +3 (black curve) and +6 (blue) (i.e., 3 months and 6 months, respectively, after an ENSO event peaks), and time series of standard deviation of Niño3.4 (red curve), calculated using a 20-year sliding window; b) and c), patterns of one-standard deviation anomalies of SST and zonal wind associated with ENSO for a strong transmission period (year 315); d) and e), the same as b) and c) but for a weak transmission period (year 215).

Figure 5. Maps of "signal to noise" ratio defined as the standard deviation of a signal over the standard deviation of noise for the coupled model (left column) and SODA-POP (right column) in terms of $D20$. See text for details. Upper row shows patterns for a strong transmission period (model year 315, and post-1980) while lower low shows those for a weak transmission period (model year 215 and pre-1980 SODA).

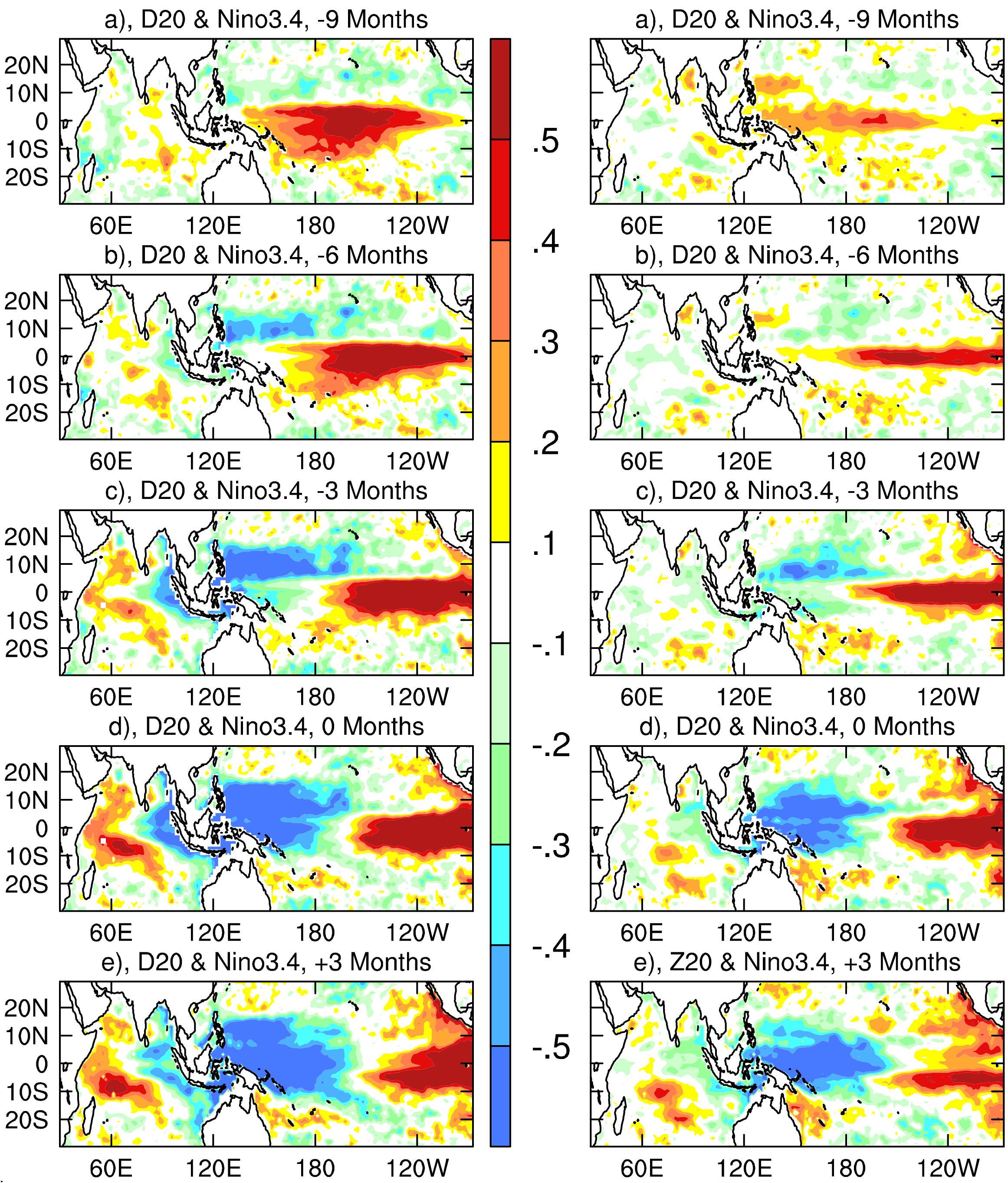

a), D20 & Nino3.4, -9 Months
b), D20 & Nino3.4, -6 Months
c), D20 & Nino3.4, -3 Months
d), D20 & Nino3.4, 0 Months
e), D20 & Nino3.4, +3 Months
a), D20 & Nino3.4, -9 Months
b), D20 & Nino3.4, -6 Months
c), D20 & Nino3.4, -3 Months
d), D20 & Nino3.4, 0 Months
e), Z20 & Nino3.4, +3 Months
20N
10N
0
10S
20S
60E
120E
180
120W
.5
.4
.3
.2
.1
-.1
-.2
-.3
-.4
-.5

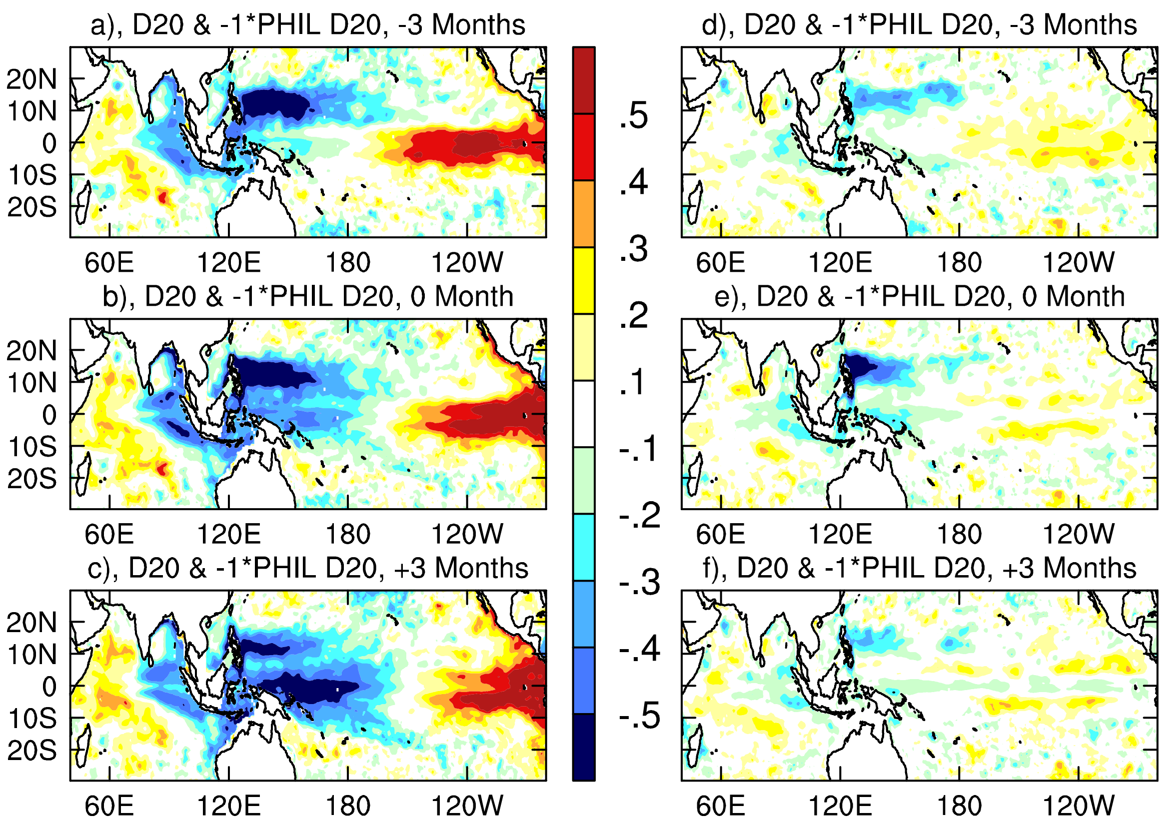

a), D20 & -1*PHIL D20, -3 Months
b), D20 & -1*PHIL D20, 0 Month
c), D20 & -1*PHIL D20, +3 Months
d), D20 & -1*PHIL D20, -3 Months
e), D20 & -1*PHIL D20, 0 Month
f), D20 & -1*PHIL D20, +3 Months
20N
10N
0
10S
20S
60E
120E
180
120W
.5
.4
.3
.2
.1
-.1
-.2
-.3
-.4
-.5

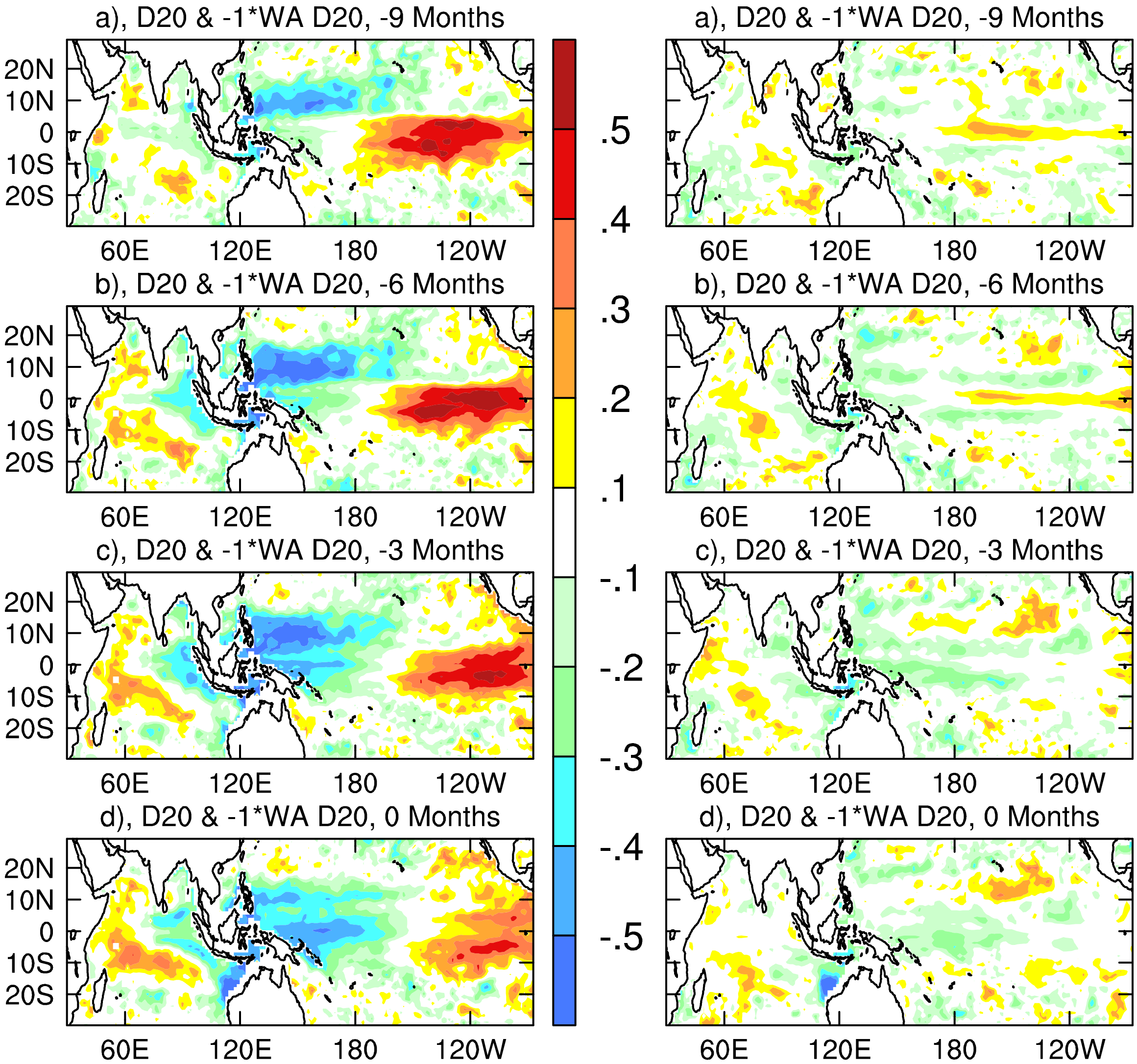
a), D20 & -1*WA D20, -9 Months
b), D20 & -1*WA D20, -6 Months
c), D20 & -1*WA D20, -3 Months
d), D20 & -1*WA D20, 0 Months
20N
10N
0
10S
20S
60E
120E
180
120W
.5
.4
.3
.2
.1
-.1
-.2
-.3
-.4
-.5

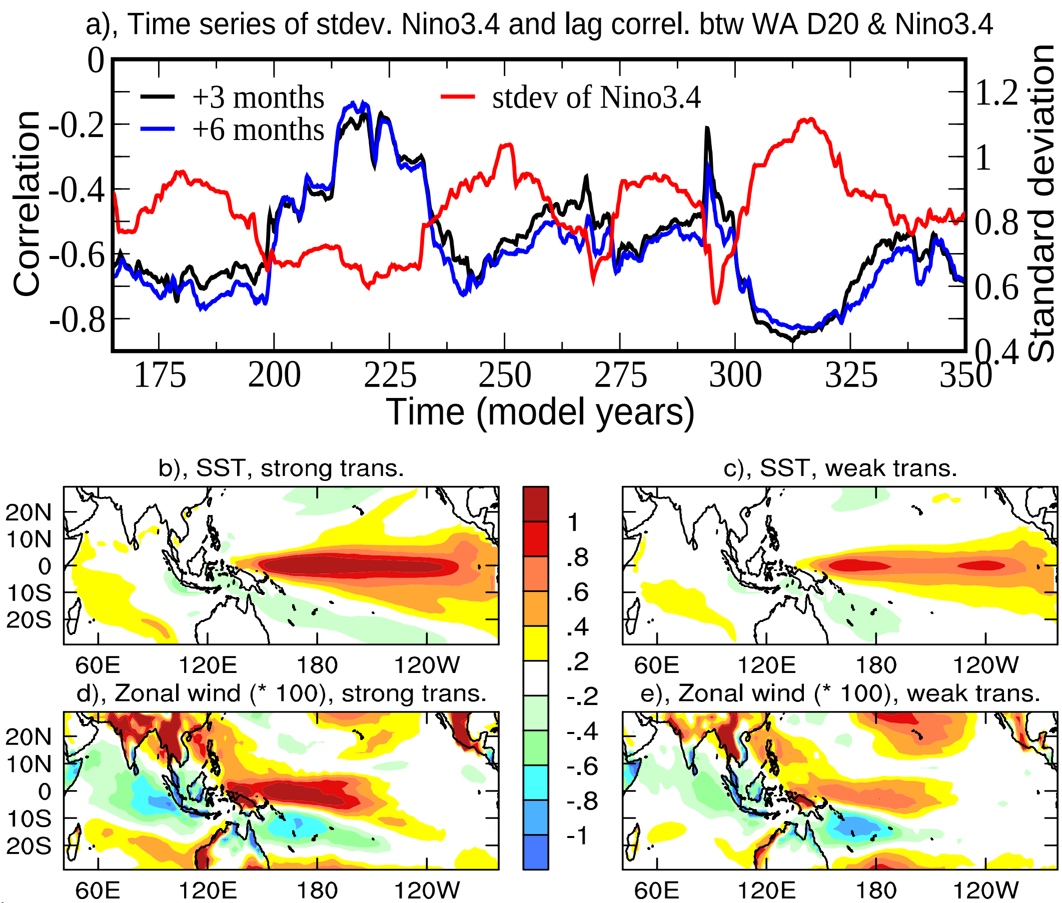
a), Time series of stdev. Nino3.4 and lag correl. btw WA D20 & Nino3.4
+3 months
+6 months
stdev of Nino3.4
Correlation
Standard deviation
Time (model years)
0
-0.2
-0.4
-0.6
-0.8
1.2
1
0.8
0.6
0.4
175
200
225
250
275
300
325
350
b), SST, strong trans.
c), SST, weak trans.
d), Zonal wind (* 100), strong trans.
e), Zonal wind (* 100), weak trans.
20N
10N
0
10S
20S
60E
120E
180
120W
1
.8
.6
.4
.2
-.2
-.4
-.6
-.8
-1

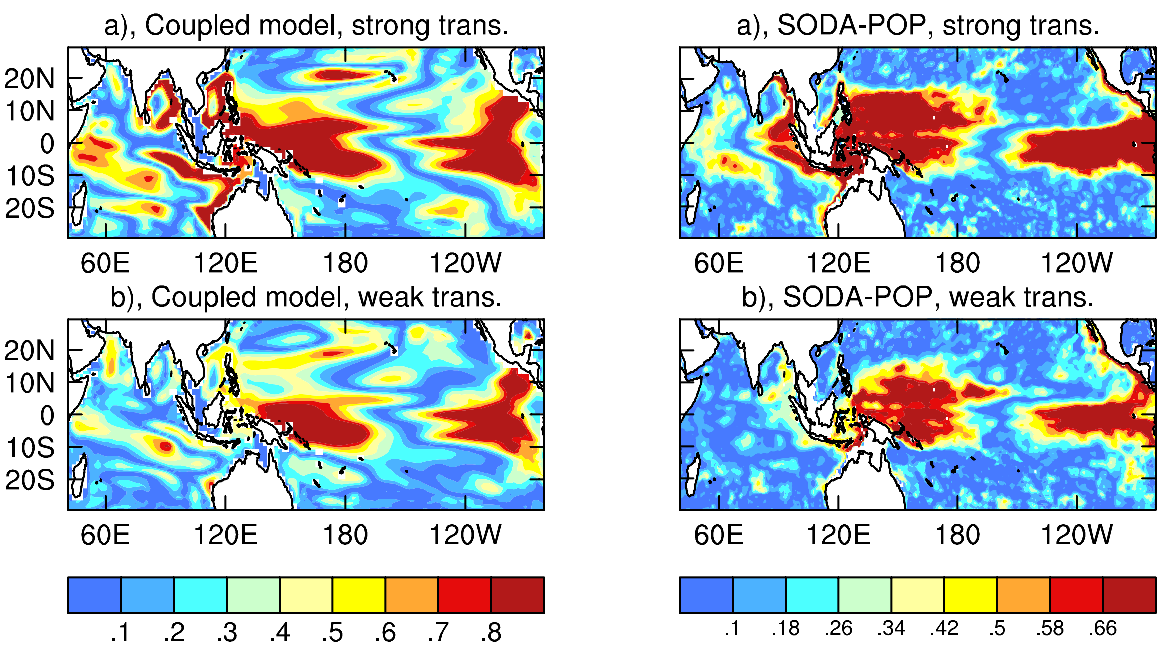
a), Coupled model, strong trans.
a), SODA-POP, strong trans.
b), Coupled model, weak trans.
b), SODA-POP, weak trans.
20N
10N
0
10S
20S
60E
120E
180
120W
.1 .2 .3 .4 .5 .6 .7 .8
.1 .18 .26 .34 .42 .5 .58 .66